Bound entanglement in thermalized states and black hole radiation: Supplemental material

Shreya Vardhan,[1] Jonah Kudler-Flam,[2] Hassan Shapourian,[3] and Hong Liu[1]

[1] *Center for Theoretical Physics, Massachusetts Institute of Technology, Cambridge, MA 02139*
[2] *Kadanoff Center for Theoretical Physics, University of Chicago, Chicago, IL 60637*
[3] *Microsoft Station Q, Santa Barbara, CA 93109*

(Dated: March 22, 2022)

I. INFORMATION-THEORETIC QUANTITIES FOR MIXED-STATE ENTANGLEMENT

Consider a state ρ in a bipartite system $\mathcal{H}_A = \mathcal{H}_{A_1} \otimes \mathcal{H}_{A_2}$. ρ is said to be a separable state if it can be written as a convex combination of product states,

$$\rho = \sum_{i=1}^{q} p_i \, (\rho_i)_{A_1} \otimes (\tilde{\rho}_i)_{A_2} \,, \quad 0 \leq p_a \leq 1, \quad \sum_{a=1}^{q} p_a = 1 \,. \tag{1}$$

Such a state has no quantum entanglement, as the correlations in it can be given a classical hidden-variable description [1], and it may be prepared using only LOCC without any need for EPR pairs between A_1 and A_2. Any state ρ that is not separable is said to be entangled.

While no general criterion is known to determine whether or not an arbitrary state ρ is entangled (doing so is an NP-hard problem [2]), we can use various quantities to study entanglement in mixed states. One familiar quantity is the mutual information

$$I(A_1, A_2) = S(\rho_{A_1}) + S(\rho_{A_2}) - S(\rho_A), \tag{2}$$

where $S(\rho)$ is the von Neumann entropy

$$S(\rho) = -\mathrm{Tr}[\rho \log \rho] \tag{3}$$

of ρ, and ρ_{A_s} in (2) refers to the reduced density matrix in subsystem A_s. While the mutual information is non-zero for any entangled state, it is also nonzero for the separable state (1) with $q > 1$, and can hence reflect both classical and quantum correlations. Note that we can also define the Rényi mutual information in terms of the n-th Rényi entropy,

$$I_n(A_1, A_2) = S_n(\rho_{A_1}) + S_n(\rho_{A_2}) - S_n(\rho_A), \quad S_n(\rho) = -\frac{1}{n-1} \log \mathrm{Tr}[\rho^n] \,, \tag{4}$$

although the physical interpretation of this quantity is not well-understood, and in particular it can take negative values.

Another useful measure is the logarithmic negativity, defined in terms of the partial transpose ρ^{T_2} of ρ, which is given by

$$\rho^{T_2}_{a_1 a_2, b_1 b_2} = \rho_{a_1 b_2, b_1 a_2} \,. \tag{5}$$

where a_1, b_1 and a_2, b_2 are indices in A_1 and A_2 respectively. In terms of the eigenvalues λ_i of $\rho_A^{T_2}$, the logarithmic negativity is defined as

$$\mathcal{E}(A_1, A_2) = \log \left(\sum_i |\lambda_i| \right) \,. \tag{6}$$

States with $\mathcal{E}(A_1, A_2) > 0$ are always entangled. States with $\mathcal{E}(A_1, A_2) = 0$ are referred to as positive partial-transpose (PPT) states, and include the entire set of separable states, but also include some (bound) entangled states.

From an operational perspective, two natural measures are the entanglement cost and the distillable entanglement. For both quantities, we take n copies of the original system, $A_1^{\otimes n} \otimes A_2^{\otimes n}$. We allow only local operations and classical communication between $A_1^{\otimes n}$ and $A_2^{\otimes n}$, and consider conversions between $\rho^{\otimes n}$ and $(|\mathrm{EPR}\rangle\langle\mathrm{EPR}|)^{\otimes m}$, where

$$|\mathrm{EPR}\rangle = \frac{1}{\sqrt{2}}(|0\rangle_{x_1}|0\rangle_{x_2} + |1\rangle_{x_1}|1\rangle_{x_2}), \quad x_1, x_2 \text{ are qubits in } A_1^{\otimes n}, A_2^{\otimes n}. \tag{7}$$

First consider the conversion from $(|\text{EPR}\rangle\langle\text{EPR}|)^{\otimes m}$ to $\rho^{\otimes n}$ under different choices $\mathcal{L}$ of LOCC operations, with vanishing error in the limit $n \to \infty$. E_c is defined as the minimum ratio $\frac{m}{n}$ over all choices of $\mathcal{L}$ [3]. We can also require that the error in the conversion vanishes before taking the $n \to \infty$ limit, and the corresponding minimum ratio $\frac{m}{n}$ is then called the exact entanglement cost $E_c^{(\text{exact})}$ [4]. Next, consider the conversion from $\rho^{\otimes n}$ to $(|\text{EPR}\rangle\langle\text{EPR}|)^{\otimes m}$ under LOCC operations $\mathcal{L}$. Now the maximum ratio $\frac{m}{n}$ over all choices of $\mathcal{L}$ is defined as the distillable entanglement E_d if we require the error to vanish only in the $n \to \infty$ limit, and the exact distillable entanglement $E_d^{(\text{exact})}$ if we require the error to vanish before taking the $n \to \infty$ limit. While for pure states ρ_A, E_c and E_d are both equal to the entanglement entropy $S(\rho_{A_1})$, for mixed states in general $E_c \geq E_d$ and neither of these quantities must be equal to $S(\rho_{A_1})$.

If we consider the set of PPT-preserving transformations (i.e. transformations that send any state σ with $\sigma^{T_2} \geq 0$ to another state σ' with $(\sigma')^{T_2} \geq 0$), of which LOCC transformations are a proper subset, then we can again consider the asymptotic rates of converting between $(|\text{EPR}\rangle\langle\text{EPR}|)^{\otimes m}$ and $\rho^{\otimes n}$ under such operations. The entanglement costs and distillable entanglements under such operations, $E_c^{(\text{ppt})}$, $E_d^{(\text{ppt})}$, $E_c^{(\text{ppt,exact})}$ and $E_d^{(\text{ppt,exact})}$ are then given by the natural generalizations of the definitions for LOCC in the previous paragraph.

It is clear from the above definitions that for a fixed set of operations, the exact costs are always greater than or equal to the costs, and the LOCC costs are always greater than or equal to the corresponding PPT costs.

While the various entanglement costs and distillable entanglements are all difficult to compute in practice, they are related to calculable measures such as I and $\mathcal{E}$ through various bounds, such as [5, 6],

$$E_d(A_1, A_2) \leq \frac{1}{2} I(A_1, A_2), \quad E_c^{(\text{ppt,exact})}(A_1, A_2) \geq \mathcal{E}(A_1, A_2). \tag{8}$$

II. EQUILIBRIUM APPROXIMATION FOR RÉNYI AND LOGARITHMIC NEGATIVITY

We consider a system evolving from a far-from-equilibrium pure state $\rho_0 = |\Psi_0\rangle\langle\Psi_0|$ to a state $\rho = |\Psi\rangle\langle\Psi|$ with $|\Psi\rangle = U|\Psi_0\rangle$, which is in equilibrium at macroscopic level. We assume that the macroscopic physical properties of the equilibrated pure state ρ can be approximated by an equilibrium density operator $\rho^{(\text{eq})}$ as in (1) from the main text.

Consider the n^{th} Rényi entropy with respect to a subsystem R,

$$\mathcal{Z}_{n,R} = e^{-(n-1)S_n^{(A)}} := \text{Tr}_R \rho_R^n = \text{Tr}_R \left(\text{Tr}_{\bar{R}} U \rho_0 U^\dagger\right)^n = \left\langle \eta_R \otimes e_{\bar{R}} | (U \otimes U^\dagger)^n | \rho_0, e \right\rangle \tag{9}$$

where in the last equality we have written this quantity as an amplitude in the replica space $(\mathcal{H} \otimes \mathcal{H})^n$, with the following notation. For any operator $\mathcal{O}$ acting on $\mathcal{H}$, the state $|\mathcal{O}, \sigma\rangle \in (\mathcal{H} \otimes \mathcal{H})^n$, where σ is an element of the permutation group $\mathcal{S}_n$ of n objects, is defined as

$$\langle i_1 \bar{i}'_1 i_2 \bar{i}'_2 \cdots i_n \bar{i}'_n | \mathcal{O}, \sigma \rangle = \mathcal{O}_{i_1 i'_{\sigma(1)}} \mathcal{O}_{i_2 i'_{\sigma(2)}} \cdots \mathcal{O}_{i_n i'_{\sigma(n)}}, \quad \mathcal{O}_{ij} = \langle i | \mathcal{O} | j \rangle \ . \tag{10}$$

Here $\{|i_1 \bar{i}'_1 i_2 \bar{i}'_2 \cdots i_n \bar{i}'_n\rangle\}$ is a basis for $(\mathcal{H} \otimes \mathcal{H})^n$, and $\sigma(i)$ denotes the image of i under σ. For $\mathcal{O}$ given by the identity operator, we will denote the states obtained in this way simply as $|\sigma\rangle$. When the system is divided into subsystems, we can similarly define states by associating different permutations to different subsystems. For example, suppose $\mathcal{H} = \mathcal{H}_A \otimes \mathcal{H}_{\bar{A}}$. Then $|\mathcal{O}, \tau_A \otimes \sigma_{\bar{A}}\rangle$ with $\tau, \sigma \in \mathcal{S}_n$ is defined as

$$\left\langle i_{1_a} i_{1_b} \bar{i}'_{1_a} \bar{i}'_{1_b} \cdots i_{n_a} i_{n_b} \bar{i}'_{n_a} \bar{i}'_{n_b} | \mathcal{O}, \tau_A \otimes \sigma_{\bar{A}} \right\rangle = \mathcal{O}_{i_{1_a} i_{1_b}, i'_{\tau(1)_a} i'_{\sigma(1)_b}} \cdots \mathcal{O}_{i_{n_a} i_{n_b}, i'_{\tau(n)_a} i'_{\sigma(n)_b}} \tag{11}$$

where $|i_{k_a}\rangle, |\bar{i}'_{k_a}\rangle$, $|i_{k_b}\rangle, |\bar{i}'_{k_b}\rangle$ respectively denote basis vectors for subsystems A and $\bar{A}$ in the k^{th} replica of $\mathcal{H} \otimes \mathcal{H}$. In (9), for the state $|\eta_R \otimes e_{\bar{R}}\rangle$, $\mathcal{O}$ is the identity operator $\mathbf{1}$, e identity permutation and η the cyclic permutation $(n, n-1, \cdots 1)$, which sends n to $n-1$, $n-1$ to $n-2$ and so on.

As explained in [7], we can find the approximate late-time value of $\mathcal{Z}_{n,R}$ in a chaotic system by inserting a physically motivated projection in (9). The projection involves the effective identity operator $\mathcal{I}_\alpha$ associated with the macroscopic equilibrium of ρ, and leads to equation (2) in the main text.

For the partial transpose partition function $\mathcal{Z}_n^{(\text{PT})}$, a similar set of steps starting from an expression for $\mathcal{Z}_n^{(\text{PT})}$ as an amplitude in $(\mathcal{H} \otimes \mathcal{H})^n$ leads to the expression equation (6) of the main text, where η^{-1} is permutation $(1\,2\,...\,n-1\,n)$. Each term in equation (6) can be given a diagrammatic representation, as shown in Fig. 1. These diagrams make it easier to understand the dependence of different terms on $\mathcal{I}_\alpha$ and the sizes of various subsystems. We can insert the

identity in the terms of equation (2) to write

$$\begin{aligned}\langle \eta_{A_1}\otimes\eta_{A_2}^{-1}\otimes e_B|\mathcal{I}_\alpha,\tau\rangle &= \sum_{i_1,i'_1,\ldots i_n,i'_n}\langle \eta_{A_1}\otimes\eta_{A_2}^{-1}\otimes e_B|i_1\bar{i}'_1\ldots i_n\bar{i}'_n\rangle\langle i_1\bar{i}'_1\ldots i_n\bar{i}'_n|\mathcal{I}_\alpha,\tau\rangle\,,\\ |i_m\rangle = |i_{m_a}\rangle_{A_1}|i_{m_{\bar{a}}}\rangle_{A_2}|i_{m_b}\rangle_B,&\quad |\bar{i}'_m\rangle = |\bar{i}'_{m_a}\rangle_{A_1}|\bar{i}'_{m_{\bar{a}}}\rangle_{A_2}|\bar{i}'_{m_b}\rangle_B\,.\end{aligned} \tag{12}$$

The lower half of each diagram represents $\langle \eta_{A_1}\otimes\eta_{A_2}^{-1}\otimes e_B|i_1\bar{i}'_1\ldots i_n\bar{i}'_n\rangle$ by connecting i_{m_a} with $i'_{\eta(m)_a}$ using dashed lines, $i_{m_{\bar{a}}}$ with $i'_{\eta^{-1}(m)_{\bar{a}}}$ using dotted lines, and i_{m_b} with i'_{m_b} using solid lines, as shown in Fig. 1(a). The upper half of the diagram represents $\langle i_1\bar{i}'_1\ldots i_n\bar{i}'_n|\mathcal{I}_\alpha,\tau\rangle$, by connecting i_m with $i'_{\tau(m)}$, as shown for some examples in Fig. 1. There is a similar diagrammatic representation for equation (2) of the main text which was explained in [7].

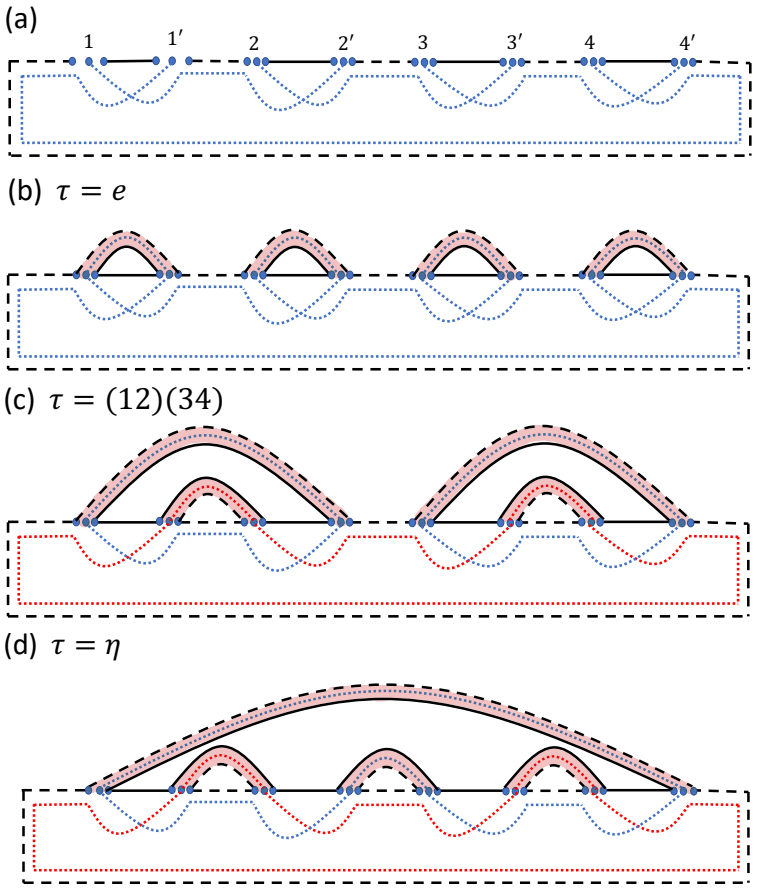

FIG. 1. (a) shows the common lines of all diagrams for different terms in equation (6) of the main text, and (b)-(d) show examples for three choices of τ which are dominant in various regimes, for the case $n = 4$. The dotted loops are shown in two different colors in (c) to make the distinction between different loops clear.

In the thermodynamic limit, the RHS of (2) and (6) of the main text can be approximated by the terms from some subset of permutations that give the dominant contribution. For the Rényi partition function (2), the dominant contribution is always given by either $\tau = e$ or $\tau = \eta$, leading to

$$S_n(\rho_R) = \min(S^{(\mathrm{eq})}_{n,R}, S^{(\mathrm{eq})}_{n,\bar{R}}) \tag{13}$$

where $S^{(\mathrm{eq})}_{n,R}$ is the n^{th} Rényi entropy of R for the state $\rho^{(\mathrm{eq})}$. For the partial transpose partition function $\mathcal{Z}^{(\mathrm{PT})}_n$ with even n, the dominant contribution for all choices of $\mathcal{I}_\alpha$ is given in different parts of the phase diagram by one out of $\tau = e$, $\tau = \eta$ or η^{-1}, and $\tau = \tau_{ES}$, where τ_{ES} refers to the two permutations with two-cycles among adjacent elements,

$$\tau_{ES} = \{(12)(34)\ldots(n-1\,n),\ (23)(45)\ldots(n\,1)\} \tag{14}$$

The diagrams corresponding to e, η and one of the permutations in τ_{ES} for $n = 4$ are shown in Fig. 1. On analytic continuation to $n \to 1$, the contributions to $\mathcal{Z}_n^{(\mathrm{PT})}$ from these permutations respectively give the finite-temperature expressions for the negativity in the NE, ME and ES phases in (16)-(18), (22)-(24), and (26)-(28) of the main text.

In gravity setups, where we take B to be the black hole subsystem and A to be the radiation, the contributions to $\mathcal{Z}_n^{(\mathrm{PT})}$ from the permutations τ_{ES}, η, and η^{-1} all involve replica wormholes. For example, consider the model for black hole evaporation in [8] where the black hole subsystem consists of JT gravity with EOW (end-of-the-world) branes. The boundary calculation of $\mathcal{Z}_n^{(\mathrm{PT})}$ between two parts of the radiation in this model is precisely equivalent to equation (6) in the main text, with effective identity operator

$$\mathcal{I}_\alpha = \mathbf{1}_A \otimes e^{-\beta H_B} f(H_B)\,. \tag{15}$$

This is a special case of equation (15) from the main text, with A at infinite temperature and an additional factor $f(H_B)$ which captures contributions from end-of-the-world (EOW) branes. In this example, we can read off the boundary expressions for $\mathcal{Z}_n^{(\mathrm{PT})}(\tau)$ in terms of $d_{A_1}, d_{A_2}, Z_{n,B}$ from the diagrams in Fig. 1 (where $Z_{n,B} = \mathrm{Tr}[(e^{-\beta H_B} f(H_B))^n]$). Using the relation between bulk and boundary partition functions in holography, we then find geometries like the ones shown in Fig. 2 for evaluating $\mathcal{Z}_n^{(\mathrm{PT})}$ in the ES and ME phases. Both involve connected Euclidean gravity path integrals between multiple asymptotic boundaries. More generally, equation (6) in the main text can be used to systematically derive replica wormhole prescriptions for calculating $\mathcal{Z}_n^{(\mathrm{PT})}$ in other gravity setups.

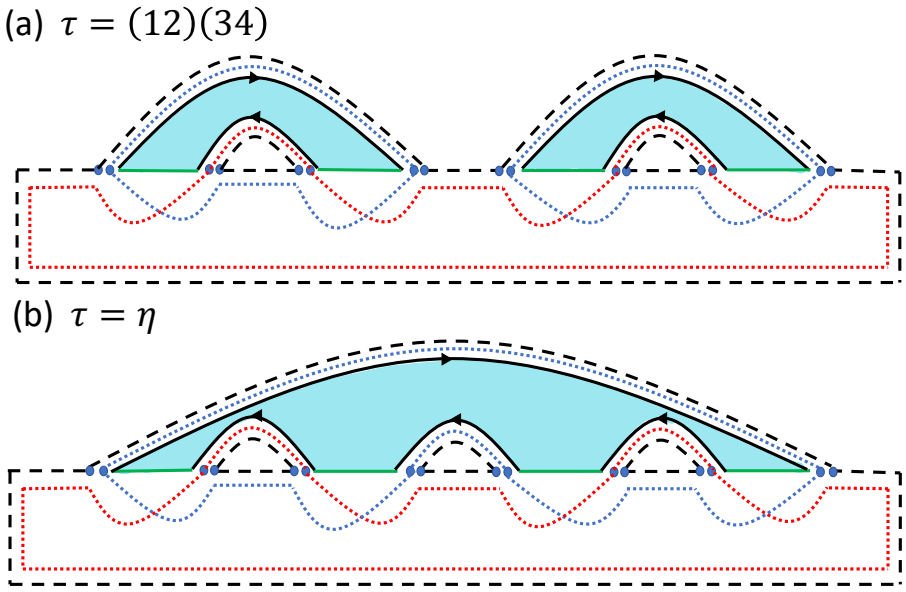

FIG. 2. Euclidean gravity path integrals with replica wormholes for calculating $\mathcal{Z}_n^{(\mathrm{PT})}$ in the model of [8], for $n = 4$. The dominant contribution in the ES phase, shown in (a), involves connected partition functions $Z_{2,B}$ between two asymptotic boundaries, while the ME phase contribution in (b) involves $Z_{n,B}$. The black lines with arrows are asymptotic boundaries in JT gravity (each with length β, although the lengths appear to differ in the figure), and the green lines are EOW branes. The dashed and dotted loops simply give factors of d_{A_1} and d_{A_2} respectively.

III. CALCULATION OF LOGARITHMIC NEGATIVITY THROUGH THE RESOLVENT

In order to find the von Neumann entropy and the logarithmic negativity, especially in the cases at finite temperature where we cannot a priori use analytic continuation, it is useful to first find the equilibrium approximation for the resolvents in equations (3) and (7) from the main text. Below we will explicitly discuss how to find R_N; the calculation for the resolvent for the von Neumann entropy is similar.

It is useful to see R_N as the trace of a matrix

$$R_{pq} = \frac{1}{\lambda}\sum_{n=0}^{\infty}\frac{1}{\lambda^n}(\rho_A^{T_2})^n{}_{pq}, \quad |p\rangle = |p_1\rangle_{A_1}|p_2\rangle_{A_2}, \quad |q\rangle = |q_1\rangle_{A_1}|q_2\rangle_{A_2} \tag{16}$$

We can apply the equilibrium approximation to each $(\rho_A^{T_2})^n{}_{pq}$. The common lower half of the diagrams for all permutations in this case can be deduced from Fig. 1 (a) for $\mathrm{Tr}[(\rho_A^{T_2})^n]$ by erasing the dashed line connecting i'_{a_n} and i_{a_1}, and the dotted line connecting $i'_{\bar{a}_1}$ and $i_{\bar{a}_n}$, and instead taking the inner product of $|i_{a_1}\rangle$, $|i'_{\bar{a}_1}\rangle$, $|i_{a_n}\rangle$, $|i'_{\bar{a}_n}\rangle$ with $|p_1\rangle$, $|p_2\rangle$, $|q_1\rangle$, $|q_2\rangle$ respectively. The resulting lines are shown in Fig. 3, which also explains how the factors of $\frac{1}{\lambda^{n+1}}$ and $\frac{1}{Z_1^n}$ that are common to all terms for a given n in (16) (the second factor comes from the equilibrium approximation) are incorporated into these lines. In the limit where the effective dimension of A_1 is much larger than

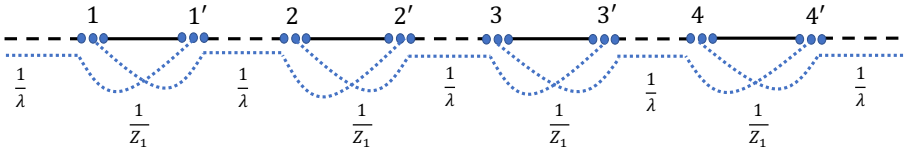

FIG. 3. "Boundary" lines for the equilibrium approximation for R_{pq} with $n = 4$.

that of A_2, it is sufficient to consider contributions from planar diagrams for all n to R_{pq}. We can write R_{pq} in terms of a self-energy Σ_{pq} as shown in Fig. 4(a). Σ_{pq} is a sum of diagrams without any disconnected parts connected by $\frac{1}{\lambda}\delta_{pq}$, to which the first few contributions are shown in Fig. 4(b). We take $|p_1\rangle, |q_1\rangle$ and $|p_2\rangle, |q_2\rangle$ to be elements of the energy eigenbasis in A_1 and A_2 respectively, so that we approximately have that

$$\langle p_1|\langle p_2|\mathcal{I}_\alpha|q_1\rangle|q_2\rangle \propto \delta_{p_1\,q_1}\,\delta_{p_2\,q_2} \tag{17}$$

for both the canonical and microcanonical ensembles, and hence from the diagrams contributing to Σ_{pq} we can see that both Σ_{pq} and R_{pq} are proportional to δ_{pq}.

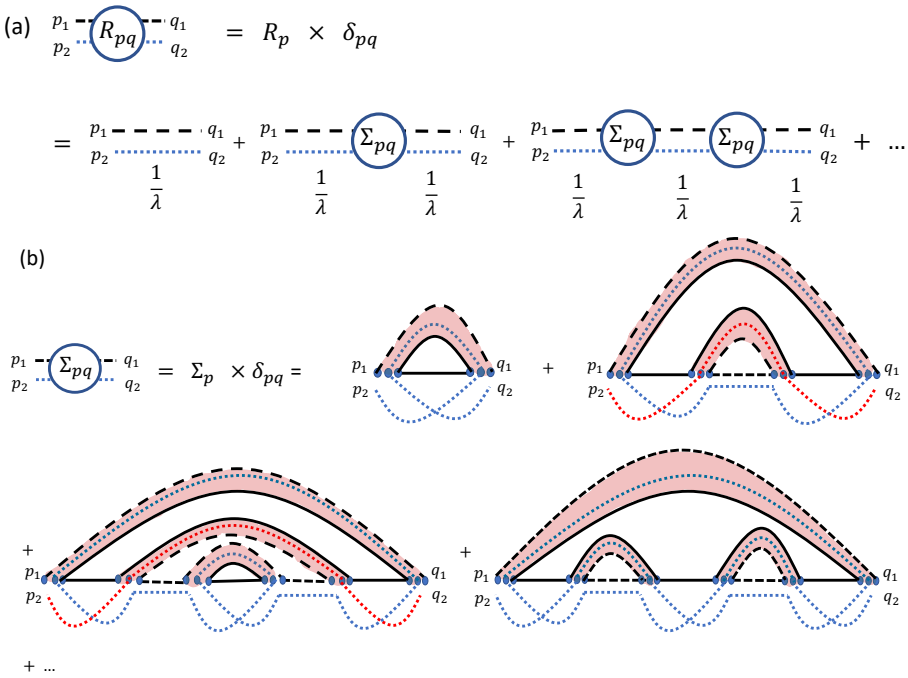

FIG. 4. Diagrammatic representation of R_{pq} and the first few diagrams contributing to Σ_{pq} in the case where A_1 is larger than A_2.

We can immediately see by summing the geometric series on the RHS of Fig. 4(a) that

$$R_N = \sum_p R_p, \quad R_p = \frac{1}{\lambda - \Sigma_p}\,. \tag{18}$$

We can systematically include all planar contributions to Σ_p using the Schwinger-Dyson equation shown diagrammatically in Fig. 5. For general choices of $\mathcal{I}_\alpha$, this Schwinger-Dyson equation in general leads to a complicated

set of equations relating R_p for all different p to each other. Below we consider a few choices of $\mathcal{I}_\alpha$ for which the Schwinger-Dyson equation simplifies. More details of each of these calculations will be discussed in [9].

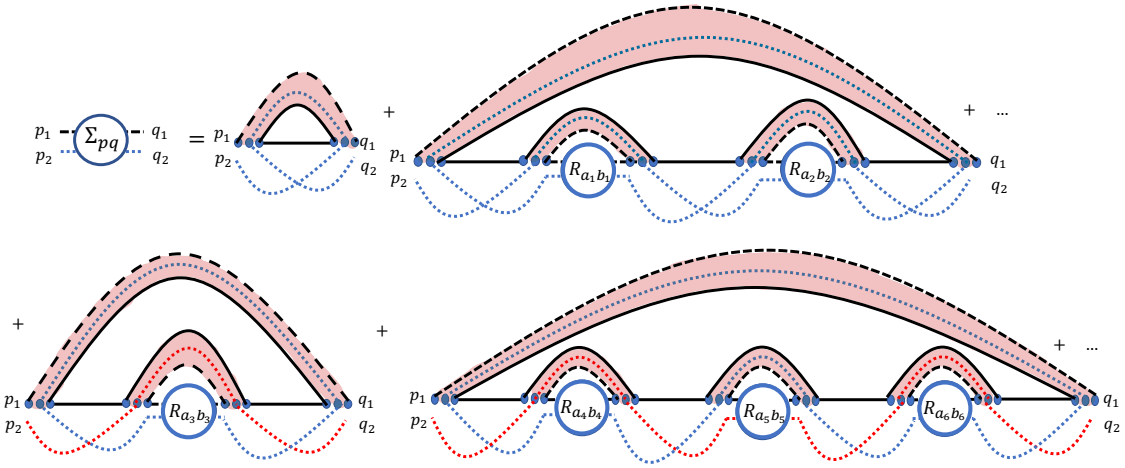

FIG. 5. Rewriting of the RHS of Fig. 4(b) as a Schwinger-Dyson equation. All a_i, b_i are independently summed over (unless they have delta functions among each other or with p, q according to the diagram).

A. Infinite temperature

Taking $\mathcal{I}_\alpha$ to be the identity operator on the full system, the Schwinger-Dyson equation for R_p becomes independent of the index p in A, and we have

$$R_N = d_A R_1, \quad R_1 = \frac{1}{\lambda - \Sigma_1}. \tag{19}$$

Each line on the RHS of Fig. 5 now simplifies to a geometric series, and we get a cubic equation for R_1,

$$\beta\lambda R_1^3 + (\alpha - \beta) R_1^2 + \left(\frac{1}{d_A} - \lambda\right) R_1 + 1 = 0, \quad \alpha = \frac{1}{d_A d_B}, \quad \beta = \frac{1}{(d_{A_2} d_B)^2}. \tag{20}$$

$D_N(\lambda)$ and $\mathcal{E}$ can be found numerically from the solution to (20), and turn out to agree with the analytic continuation in equations (11)-(13) from the main text, as discussed in [10].

Now consider the regime where $d_{A_1}/(d_{A_2} d_B) \ll 1$. This corresponds to being outside the ME phase. Then since in this regime $\alpha \gg \beta$, R_1 is $O(1)$, and λ is $O(1/d_A)$, (20) simplifies to a quadratic equation for R_1,

$$\alpha R_1^2 + \left(\frac{1}{d_A} - \lambda\right) R_1 + 1 = 0. \tag{21}$$

The same quadratic equation can be obtained diagrammatically by ignoring all contributions to the Schwinger-Dyson equation in Fig. 5 except the first term in each line on the RHS. This corresponds to including contributions to $\mathcal{Z}_n^{(\mathrm{PT})}$ for all n from permutations where all cycles have either one or two elements (including $\tau = e$ and $\tau = \tau_{ES}$, as well as other permutations such as (12)). We can now solve (21) to get a simple semicircle form of $D_N(\lambda)$ from $R_N(\lambda)$, which can be integrated analytically to get the NE phase and the ES phase, and the correct transition line between them at $c = \frac{1}{2}$. But as expected, this approximation misses the ME phase.

B. Canonical ensemble with infinite temperature in A

Next, consider $\mathcal{I}_\alpha$ as in equation (15) from the main text, with infinite temperature in A. For this case, the RHS of Fig. 5 implies that R_p, Σ_p again become independent of the index p, so that we have (19) again, but now with Σ_1

dependent on the partition functions $Z_{n,B} = \mathrm{Tr}[e^{-n\beta H_B}]$. We find for this case

$$\lambda R_N = d_A + d_{A_2} \int dE \rho(E) \sum_{k=1}^{\infty} \left[\left(\frac{R_N e^{-\beta E}}{d_A d_{A_2} Z_{1,B}} \right)^{2k-1} + d_{A_2} \left(\frac{R_N e^{-\beta E}}{d_A d_{A_2} Z_{1,B}} \right)^{2k} \right]. \tag{22}$$

We then complete the geometric sums to find

$$\lambda R_N = d_A + \int dE \rho(E) \frac{d_{A_2}^2 R_N \left(d_A Z_{1,B} e^{\beta E} + R_N \right)}{d_A^2 d_{A_2}^2 Z_{1,B}^2 e^{2\beta E} - R_N^2}. \tag{23}$$

where $\rho(E) = e^{Vs(E/V)}$ is the density of states for B. On specifying the density of states, this equation can be can be solved numerically for $R_N(\lambda)$ and used to obtain $\mathcal{E}$. The solution with a gaussian entropy density is shown in Fig. 6 (a) as a function of c at $\lambda = \frac{1}{2}$. The result agrees with the expressions for $\mathcal{E}$ in the ME and ES phases in equations (16) and (18) from the main text and the naive phase transition line between them in equation (19).

Similar to the infinite temperature case, we can obtain an analytic expression for the regime where the effective dimensions d_{A_1}, d_{A_2}, d_B of the different subsystems are such that $\frac{d_{A_1}}{d_{A_2} d_B} \ll 1$. Assuming that the same set of permutations contributes in this regime at finite temperature as the one that contributed at infinite temperature, we can then include only the first diagram from each line on the RHS of Fig. 5. We again find a semicircle form of $D_N(\lambda)$, which can be integrated analytically to get equations (16) and (18) and the transition (19) from the main text. But note that in this case we do not have a systematic way of justifying the truncation to the permutations with cycles of only length one and two, so it is important to confirm these expressions numerically using the full resolvent as in Fig. 6 (a).

Analogously to the above steps, we may find an integral expression for the resolvent for the von Neumann entropy of ρ_{A_1}

$$\lambda \mathcal{R} = d_{A_1} + \int dE \rho(E) \sum_{k=1}^{\infty} \left(\frac{\mathcal{R} e^{-\beta E}}{d_A Z_{1,B}} \right)^k = d_{A_1} + \int dE \rho(E) \frac{\mathcal{R}}{d_A Z_{1,B} e^{\beta E} - \mathcal{R}}. \tag{24}$$

The von Neumann entropy can again be evaluated numerically, confirming the expectation from analytic continuation in equation (14) of the main text, as shown in Fig. 6 (b).

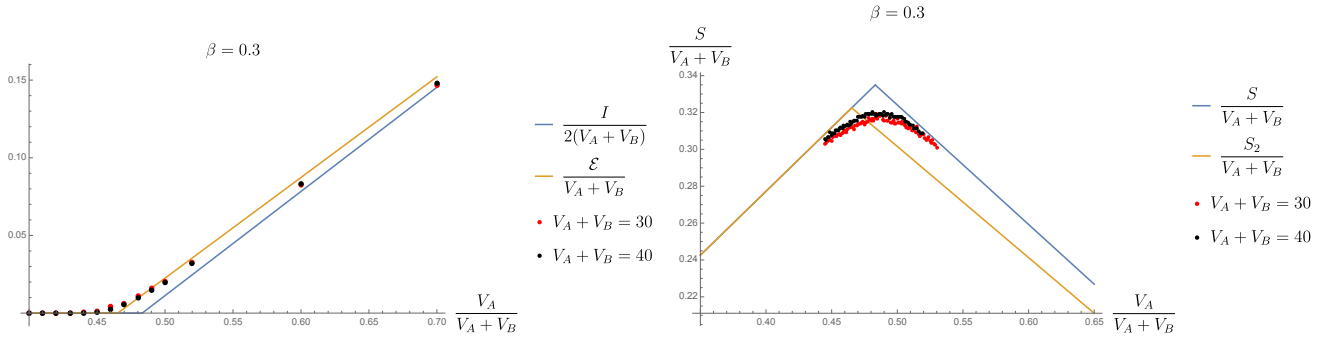

FIG. 6. Left: For the canonical ensemble with A at infinite temperature, the logarithmic negativity is computed numerically using the resolvent (23) and compared to the naive analytic continuation in equations (16) and (18) from the main text, with excellent agreement. Right: The same is done for the von Neumann entropy of $A_1 = A$ using the resolvent (24). Clearly, the Page transition occurs at the same place as the naive analytic continuation in equation (14) of the main text and not at, for instance, the transition for the second Rényi entropy. For simplicity, we have used a Gaussian density of states $\rho(E) \propto \exp\left[-\frac{E^2}{2N_B}\right]$ and taken $\lambda = \frac{1}{2}$.

C. Microcanonical ensemble with B at infinite temperature

In this case, R_p is no longer independent of p, but instead depends on the energies of $|p_1\rangle, |p_2\rangle$. The resolvent calculation for this case becomes more complicated, and we are not able to find $\mathcal{E}$ from the sum over all permutations either analytically or numerically. But if we again truncate to the contributions from permutations that have cycles

with only one and two elements, assuming this truncation is valid away from the ME phase, then this results in a form of $D_N(\lambda)$ which can be integrated analytically to confirm equations (22) and (24) from the main text. The naive transition line where we set equation (24) to zero is also confirmed by this calculation.

D. Microcanonical ensemble with A_2 at infinite temperature

In this case, the expressions for $\mathcal{Z}_n^{(\mathrm{PT})}$ are such that the resolvent can be expressed in a simple way in terms of the infinite-temperature resolvent from (20). As a result, the quantity $\mathcal{Z}^{(\mathrm{PT})} \equiv \exp \mathcal{E}$ can also be expressed in a simple way in terms of its infinite temperature value $\mathcal{Z}_\infty^{(\mathrm{PT})}(d_{A_1}, d_{A_2}, d_B)$,

$$\mathcal{Z}^{(\mathrm{PT})} \approx \sum_{E_1} p_{E_1}\, \mathcal{Z}_\infty^{(\mathrm{PT})}(d_{E_1}^{A_1},\, d_{A_2},\, d_{E-E_1}^{B}) \tag{25}$$

where $d_{E_R}^R \equiv e^{V_R\, s(E_R/V_R)}$ refers to the density of states in subsystem R at energy E_R, with $s(\epsilon)$ the entropy density for the system, and

$$p_{E_1} = \frac{d_{E_1}^{A_1} d_{E-E_1}^{B}}{N_E}, \quad N_E = \sum_{E_1'} d_{E_1'}^{A_1} d_{E-E_1'}^{B}\,. \tag{26}$$

In the thermodynamic limit, for certain ranges of c and λ, (25) gives the expressions expected from analytic continuation in equations (26)-(28) from the main text. In addition to these, we get two new phases, where

$$\mathcal{E}_{ES-ME1} = \log d_{A_2} + V_{A_1}(s(\theta_3) - s(\epsilon)) - V_B s(\epsilon)\,. \tag{27}$$

$$\mathcal{E}_{ES-ME2} = V_{A_1}\,(2s(\theta_2) - s(\epsilon)) - V_B\, s(\epsilon)\,. \tag{28}$$

with $\epsilon = \frac{E}{V_{A_1}+V_B}$, and θ_2 and θ_3 defined implicitly as solutions to the equations

$$\begin{aligned} \log d_{A_2} + V_B\, s\left(\frac{\epsilon\,(V_{A_1}+V_B) - V_{A_1}\,\theta_2}{V_B}\right) &= V_{A_1} s(\theta_2), \\ V_{A_1}\, s(\theta_3) + V_B\, s\left(\frac{\epsilon\,(V_{A_1}+V_B) - V_{A_1}\,\theta_3}{V_B}\right) &= \log d_2\,. \end{aligned} \tag{29}$$

The full phase diagram is shown in Fig. 3 of the main text.

[1] R. F. Werner, Quantum states with Einstein-Podolsky-Rosen correlations admitting a hidden-variable model, Phys. Rev. A **40**, 4277 (1989).
[2] L. Gurvits, Classical complexity and quantum entanglement, Journal of Computer and System Sciences **69**, 448 (2004).
[3] P. M. Hayden, M. Horodecki, and B. M. Terhal, The asymptotic entanglement cost of preparing a quantum state, Journal of Physics A Mathematical General **34**, 6891 (2001), arXiv:quant-ph/0008134 [quant-ph].
[4] Q. Yue and E. Chitambar, The zero-error entanglement cost is highly non-additive, Journal of Mathematical Physics **60**, 112204 (2019), arXiv:1808.10516 [quant-ph].
[5] M. Christandl and A. Winter, "Squashed entanglement": An additive entanglement measure, Journal of Mathematical Physics **45**, 829 (2004), arXiv:quant-ph/0308088 [quant-ph].
[6] K. Audenaert, M. B. Plenio, and J. Eisert, Entanglement Cost under Positive-Partial-Transpose-Preserving Operations, Phys. Rev. Lett. **90**, 027901 (2003), arXiv:quant-ph/0207146 [quant-ph].
[7] H. Liu and S. Vardhan, Entanglement entropies of equilibrated pure states in quantum many-body systems and gravity, arXiv e-prints , arXiv:2008.01089 (2020), arXiv:2008.01089 [hep-th].
[8] G. Penington, S. H. Shenker, D. Stanford, and Z. Yang, Replica wormholes and the black hole interior, arXiv e-prints , arXiv:1911.11977 (2019), arXiv:1911.11977 [hep-th].
[9] S. Vardhan, J. Kudler-Flam, H. Shapourian, and H. Liu, Mixed-state entanglement and information recovery in thermalized states and evaporating black holes, arXiv e-prints , arXiv:2112.00020 (2021), arXiv:2112.00020 [hep-th].
[10] H. Shapourian, S. Liu, J. Kudler-Flam, and A. Vishwanath, Entanglement Negativity Spectrum of Random Mixed States: A Diagrammatic Approach, PRX Quantum **2**, 030347 (2021), arXiv:2011.01277 [cond-mat.str-el].